Athens, and therefore, the majority of the image was textured, with a forest in the city whose boundary we wanted to find.

VI. Discussion and Conclusions

We have presented an algorithm that can locate boundaries of the textured regions, irrespective of the nature of the texture. The algorithm simply exploits the fact that a textured region has a high density of edge pixels associated with it.

The most critical stage of the algorithm is probably the edge detection stage. If we use a large edge detection filter that performs a lot of smoothing, the density of the edge points in the textured regions will not be high enough, and no sufficient differentiation will be possible between textured and non textured regions. In addition, for less well-defined textures, one will have to use larger neighborhoods in calculating the free angle at the expense of preserving the detail of the boundary. We found that the algorithm performed at its best when using Sobel edge detector in conjunction with SPOT panchromatic images.

A less critical stage of the algorithm is that of the erosion and dilation. Erosion is needed in order to remove all edge points not associated with textured regions, and by looking at Fig. 2(c) and (d), we see that just a few pixels in the textured region to the left of the center of the image that survived the erosion stage expand to form sizable regions on dilation. The erosion neighborhood, therefore, determines the minimum size of a textured region that can be located by the algorithm. The dilation neighborhood, on the other hand, has to be larger than the erosion neighborhood, although not much larger. The point is that the pixels closest to the boundary of the textured region after erosion are just beyond the size of the erosion neighborhood away from the true boundary. The dilation neighborhood therefore needs to be larger in order to restore the true boundary pixels to the region. The amount by which these two neighborhoods should differ depends on the densities of the edge pixels in the textured region. However, if one gets this wrong, the only loss will be a slightly smaller textured region. It is not advisable to reduce the sizes of the structuring elements too much as this will result in a larger number of small islands of texture being identified [12]. The size of the erosion neighborhood needs to be fixed by the scale of the texture.

In any case, note that all the results presented here have been obtained with more or less the same parameter settings. As an aside, this algorithm can be used to identify the convex hull of 2-D sets of points by setting the threshold of the free angle to 8.0.

References

[1] N. Ahuja, "Dot pattern processing using Vornoi neighborhoods," *IEEE Trans. Pattern Anal. Machine Intel.*, vol. PAMI-4, pp. 336–343, May 1982.

[2] D. G. Corr *et al.*, "Progress in automatic analysis of multi-temporal remotely-sensed data," *Int. J. Remote Sensing*, vol. 10, pp. 1175–1195, 1989.

[3] P. A. Devijver, "Selection of prototypes for nearest neighbor classification," in *Proc. Indian Stat. Inst. Golden Jubilee Int. Conf. Advances Inform. Sci. Tech.*, vol. I: *Pattern Recogn. Dig. Techn.*, 1982, pp. 84–106.

[4] P. G. Ducksbury, "Parallel texture region segmentation using a pearls Bayes network," in *British Machine Vision Conf.*, Guildford, U.K., Sept. 1993, pp. 187–196.

[5] H. Edelsbruner, D. Kirkpatrick, and R. Seidel, "On the shape of a set of points in the plane," *IEEE Trans. Inform. Theory*, vol. IT-29, pp. 551–559, July 1983.

[6] J. Fairfield, "Contoured shape generation: Forms that people see in dot patterns," *Proc. IEEE Conf. Syst., Man, Cybern.*, 1979, pp. 60–64.

[7] V. Di Gesu and M. C. Maccarone, "Description of fuzzy images by convex hull technique," in *Proc. 8th IEEE Int. Conf. Patt. Recogn.*, Paris, Oct. 1986, pp. 1276–1278.

[8] P. E. Hart, "The condensed nearest neighbors rule," *IEEE Trans. Inform. Theory*, vol. IT-14, pp. 515–516, May 1968.

[9] D. Janković, S. Matić, and V. Živojnović "On a method of finding contour prototypes for nonparametric classification," in *Proc. IEEE Int. Symp. Inf. Theory*, Ann Arbor, MI, Oct. 1986, pp. 137–143.

[10] D. Janković and J. Sklansky, "Finding contour points of an N-dimensional point cloud," Tech. Rep., Dept. Elect. Eng., Univ. California, Irvine, 1990.

[11] R. A. Jarvis, "Computing the shape hull of points in the plane," in *Proc. IEEE Comput. Soc. Conf. Pattern Recogn. Image Proc.*, Long Beach, CA, 1977, pp. 231–241.

[12] K. Krishnasamy and M. Petrou, "The Identification of textured region boundaries," in *Brit. Machine Vision Conf.*, York, U.K., 1994, pp. 125–134.

[13] J. Le Moigne and J. C. Tilton, "Refining image segmentation by integration of edge and region data," *IEEE Trans. Geosci. Remote Sensing*, vol. 33, pp. 605–615, May 1995.

[14] J. F. O'Callaghan, "Computing the perceptual boundaries of dot patterns," *Comput. Graph. Image Processing*, vol. 3, pp. 141–162, 1974.

[15] ____, "Human perception of homogeneous dot patterns," *Perception*, vol. 3, pp. 33–45, 1974.

[16] G. Toussaint, "Pattern recognition and geometric complexity," *Proc. 5th IEEE Int. Conf. Pattern Recognition*, Miami Beach, FL, Dec. 1980, pp. 1324–1347.

[17] M. Tuceryan and N. Ahuja, "Extracting perceptual structure in dot patterns: An integrated approach," Tech. Rep. IULU-ENG-87-2206, Univ. Illinois, Urbana-Champaign, Jan. 1987.

[18] F. Wang, "Knowledge-based vision system for detecting land changes at urban fringes," *IEEE Trans. Geosci. Remote Sensing*, vol. 31, pp. 136–145, Jan. 1993.

[19] S. W. Zucker and R. A. Hummel, "Toward a low-level description of dot clusters: Labeling edge, interior, and noise points," *Comput. Graph. Image Processing*, vol. 9, pp. 213–233, 1979.

The Monopole-Antenna: A Practical Snow and Soil Wetness Sensor

A. Denoth

***Abstract*—As an alternative to TDR or capacitive sensors, a monopole antenna has been tested for field measurements of liquid water content in both soil and snow. The frequency of operation is in the range of 100 MHz up to 2 GHz. Comparative field measurements of wetness profiles at snow-soil interfaces are shown.**

***Index Terms*—Monopole antenna, soil, snow, wetness.**

I. Introduction

Commonly used techniques for soil wetness measurements are the thermo-gravimetric method, neutron thermalization and TDR; calorimetric methods or capacitive sensors are applied for snow wetness detection. A comparison of the error surfaces of the various methods shows, that the highest accuracy under field conditions can be achieved by high-frequency dielectric measurements [1]; in

Manuscript received September 19, 1995; revised March 5, 1997.

The author is with the Institute of Experimental Physics, University of Innsbruck, Innsbruck A-6020, Austria (e-mail: Armin.Denoth@uibk.ac.at).

Publisher Item Identifier S 0196-2892(97)05521-6.

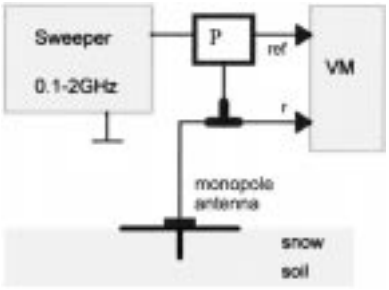

(a)

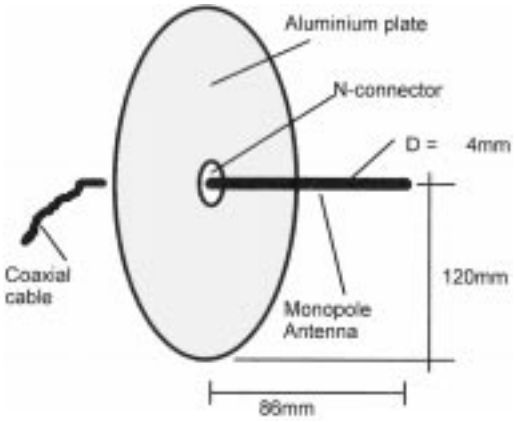

(b)

Fig. 1. (a) Schematic diagram of the monopole probe system. P: Power splitter, VM: Vector voltmeter, r: reflected signal, ref: reference signal, and (b) geometrical dimensions of the monopole antenna.

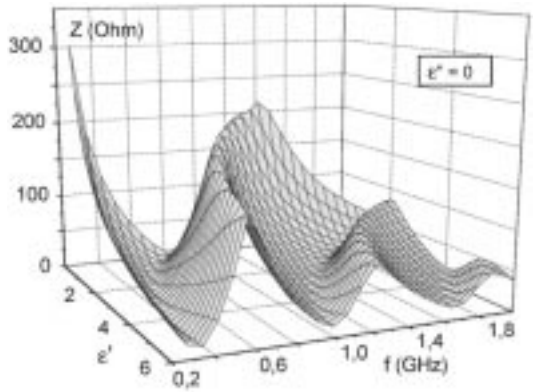

Fig. 2. Antenna input impedance as a function of frequency and snow permittivity ε', computed for constant losses $\varepsilon'' = 0$.

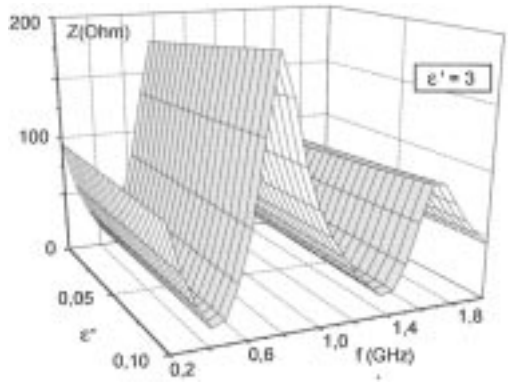

Fig. 3. Antenna input impedance as a function of frequency and snow total losses ε'', computed for constant permittivity $\varepsilon' = 3$.

addition, the dielectric sensors allow a more or less nondestructive wetness detection in geophysical materials with high spatial resolution and accuracy [2], [3]. An interesting alternative to TDR or capacitive sensors may be the monopole-antenna [4]. Its simple construction allows an easy application to grainy geophysical materials as snow or soils. An application of monopole probes for measuring dielectric properties of low-permittivity liquids has been described by Olson and Iskander [5]; Freundorfer *et al.* [6] derived soil electromagnetic properties from measurements of the radial distribution of the electric field of the antenna.

II. Experimental Setup

The experimental setup consists of a simple high-frequency vector voltmeter, a sweeper oscillator and the monopole-antenna as dielectric sensor. Measurement quantity is the driving-point impedance of the sensor; it depends on the actual geometrical dimensions of the antenna and the complex permittivity of the surrounding medium [7], and the frequency of operation. A block diagram of the experimental setup and a sketch of sensor geometry is given in Fig. 1(a) and (b).

The dielectric function of snow or soils is derived from the measured antenna impedance (Z) by matching (least-square fit) the magnitude and phase of a calculated impedance, according to [5]. As the effective antenna length, l_{eff}, and thickness, D_{eff}, may deviate slightly from the actual geometrical dimensions, these parameters have been derived from a calibration measurement of antenna driving-point impedance in air ($\varepsilon = 1$): $l_{eff} = 88$ mm, $D_{eff} = 4$ mm. The monopole antenna is operated in the frequency range from $\approx$100 MHz up to $\leq$600 MHz (for soils) and from 200 MHz to $<$2 GHz (for snow), whereby the lower limits are due to the validity of the driving-point impedance expression [5]. In addition, in the frequency range selected, snow is practically a lossless dielectric material, and soils—if not extremely wet—can be considered as substances with relatively low complex permittivities. The expected variation of antenna impedance (magnitude) with frequency, permittivity ε' and total losses ε'' is shown in Figs. 2 and 3, respectively, when applied to snow, and in Figs. 4 and 5, respectively, when applied to soils. Figs. 2 and 4 show the variation of antenna impedance surface with ε', computed for constant losses ε'' (snow: $\varepsilon'' = 0$; soil: $\varepsilon'' = 2$); Figs. 3 and 5 show the variation of impedance surface with ε'', computed for constant permittivity ε' (snow: $\varepsilon' = 3$, soil: $\varepsilon' = 15$). The range of (complex) permittivities used to calculate impedance surfaces covers the range of permittivities of natural soils and snow. Applied to soils (Figs. 4 and 5), antenna impedance shows marked variations with frequency and complex permittivity; so, the monopole probe allows the determination of both the dielectric function $\varepsilon'(f)$ and the total losses $\varepsilon''(f)$ of soils with sufficient accuracy. Applied to snow, sensor impedance is very sensitive to the permittivity ε' (Fig. 2), the effect of the comparable low dielectric losses ($\varepsilon'' < 0.05$) on sensor impedance, however, is very weak (Fig. 3), so ε'' of snow cannot be determined (in the frequency range selected) with this type of sensor. If the material is inhomogeneous, which is normally the case for natural soils or snow, only "effective" permittivities can be derived: the effective permittivity is a mean permittivity averaged over a specific measuring volume, the sphere of influence. This measurement volume depends basically on the antenna geometry (and the upper limit of measurement frequency); it can roughly be approximated by a cylinder of length L and radius R. Length and radius have been

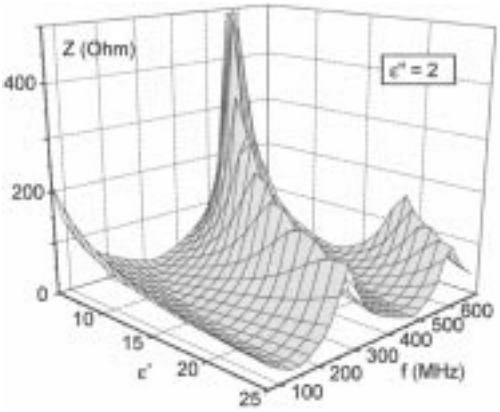

Fig. 4. Antenna input impedance as a function of frequency and soil permittivity ε', computed for constant losses $\varepsilon'' = 2$.

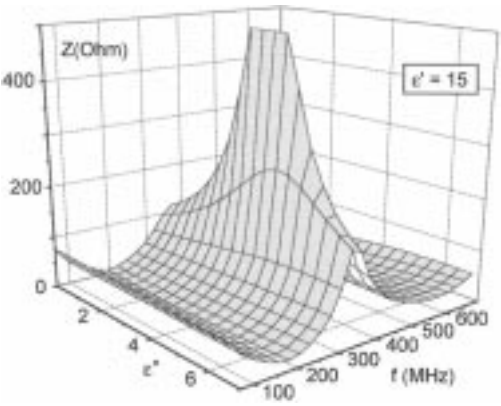

Fig. 5. Antenna input impedance as a function of frequency and soil total losses ε'', computed for constant permittivity $\varepsilon' = 15$.

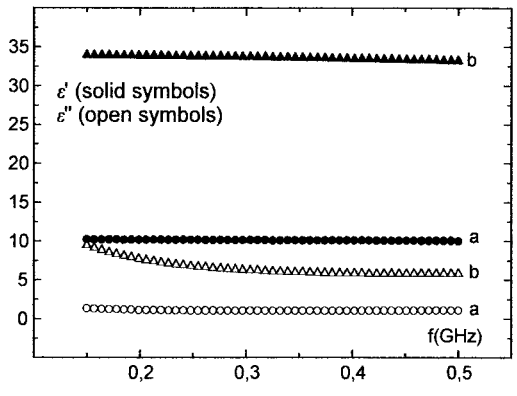

Fig. 6. Field measurements of soil dielectric function: (a) thermo-gravimetric wetness $W = 15.2\%$ and (b) $W = 43\%$. Soil characteristics: soil under pasture.

estimated experimentally $L \cong 13$ cm, and $R \cong 4$ cm; so the effective volume of the test material, which makes the dominant contribution to the measured permittivity, is approximately 650 cm^3.

III. Retrieval of Dielectric Data and Water Content

In order to test the sensor applicability for *in situ* wetness determinations, field measurements of the dielectric function of various soils (Alpine rankers, soil under pasture), and of a natural snow cover have been made. The relation between snow or soil incremental permittivity (real part) and wetness (volume basis) has been

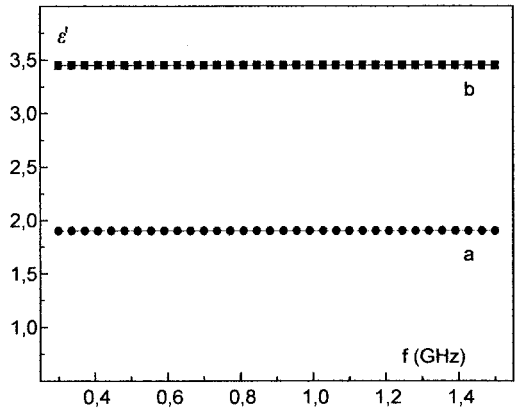

Fig. 7. Field measurements of snow dielectric function: (a) dry Alpine winter-snow and (b) Alpine old spring-snow, wetness $W = 5.8\%$.

determined experimentally. Soil wetness has been measured using both the standard thermo-gravimetric method [8] and a recently developed capacitive sensor [9], [10]; snow wetness, however, has been determined using standard calorimetric techniques (freezing calorimeter) and a calibrated capacitive sensor [11], [12]:

$$\Delta\varepsilon'(\text{snow}) = 0.186\,\text{W} + 0.0045\,\text{W}^2 \quad (10\,\text{MHz} \le f < 2\,\text{GHz})$$

$$\Delta\varepsilon'(\text{soil}) = 0.581\,\text{W} + 0.0054\,\text{W}^2 \quad (30\,\text{MHz} \le f < 200\,\text{MHz})$$

$\Delta\varepsilon'$, the incremental permittivity, reflects the increase in permittivity due to the liquid water component present: $\varepsilon'(\text{wet}) = \varepsilon'(\text{dry}) + \Delta\varepsilon'$. At the selected relatively high measurement frequencies no significant influence of soil type or stage of metamorphism of snow has been detected. $\varepsilon'(\text{dry})$, the permittivity in the "dry" condition, depends strongly on porosity; it ranges from 2.5 to 5 for soils [13], [14], and from ≈1.4 to 2.2 for snow [11]. The dielectric function of snow or soils is derived from the measured antenna impedance by a least-square fit of the magnitude and phase of a calculated impedance, according to [5], with ε' and ε'' as fit parameters. The relative errors in the determination of ε' and ε'', $E(\varepsilon')$ and $E(\varepsilon'')$, respectively, are typically less than $E < 5\%$.

Results of typical field measurements of dielectric data (ε' and ε'') are given in Fig. 6 for two soil samples of different wetness (soil characteristics: soil under pasture; $W = 15.2\%$ and $W = 43\%$, respectively) and in and Fig. 7 for a dry Alpine winter snow (density $\rho = 0.41$ g/cm^3, data ponts: solid circles) and for a moderate wet Alpine old spring-snow sample ($W = 5.8\%$, density $\rho = 0.58$ g/cm^3, data ponts: solid squares), respectively. Permittivity ε' of the very wet soil ($W = 43\%$, data ponts: solid triangles) shows a slight decrease with increasing frequency whereas the total losses (ε'', data ponts: open triangles) decrease significantly with frequency and approach a nearly constant value in the range of 400–500 MHz. This behavior of the dielectric function indicates a relaxation regime in the lower GHz-range, which has also be found by Hoekstra and Delaney [15]. The dielectric function of the moderate wet soil ($W = 15.2\%$, data ponts: solid/open circles) and of the snow samples (Fig. 7) show no significant variation with frequency. The dielectric losses of the material "snow," however, were very low; only an upper limit was estimated: $\varepsilon'' \le 0.02$.

Results for comparative liquid water measurements are given in Fig. 8. Data points represent the mean value of typically 3 up to 5 consecutive wetness determinations. Snow or soil wetness (volume basis) has been measured by the monopole probe, W(MP),

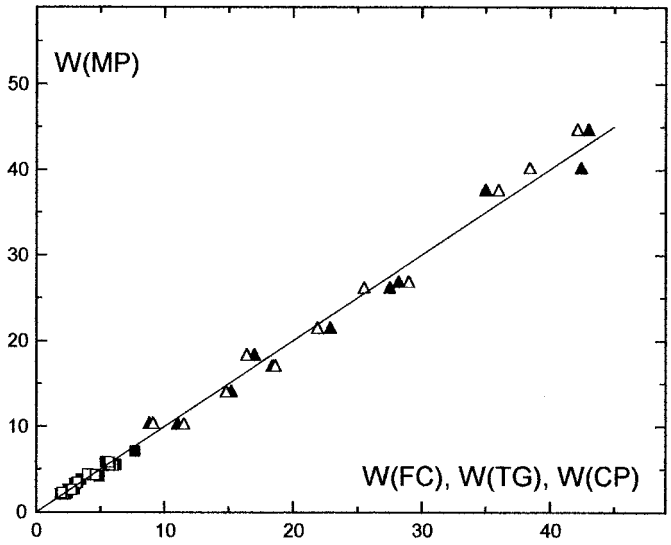

Fig. 8. Snow/soil wetness results obtained with the monopole probe, W(MP), compared to: freezing calorimetry [W(FC), solid squares], thermogravimetry [W(TG), solid triang-les], and capacitive probes [W(CP), open squares (snow), open triangles (soil)], respectively.

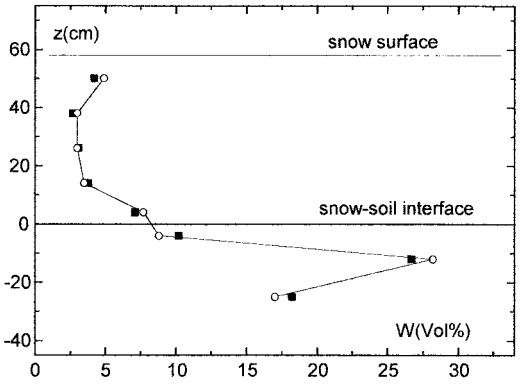

Fig. 9. Comparative measurement of a wetness profile at a snow-soil interface. Open circles: calorimetric (snow) and gravimetric (soil) measurements; solid squares: monopole-probe.

by capacitive probes, W(CP), and by the direct methods freezing calorimetry, W(FC), and thermo-gravimetry, W(TG). With regard to to the different measurement volumes (spheres of influence) of the individual sensors, measurements have been done on more or less homogeneous snow or soil samples. This comparative study shows a good agreement between the individual test series; correlation coefficient, r, and standard deviation σ have been computed for the material "snow": MP compared to FC $r = 0.977$, $\sigma = 0.33$, MP compared to CP $r = 0.984$, $\sigma = 0.27$; and for the material "soils": MP compared to TG $r = 0.990$, $\sigma = 1.74$, and MP compared to CP $r = 0.992$, $\sigma = 1.53$.

IV. Comparative Field Measurements

As a practical field application of this sensor comparative measurements of wetness profiles at snow-soil interfaces and at an internal interface of a snowcover (ice crust) are shown for different snow/soil conditions in Figs. 9, 10, and 11, respectively. Due to the relative low spatial resolution of the monopole-probe, data points have been taken only every 10–15 cm (depending on the local snow or soil structure characteristics) and are compared to calorimetric (snow), gravimetric (soil) and high-resolution capacitive (snow and soil) [9],

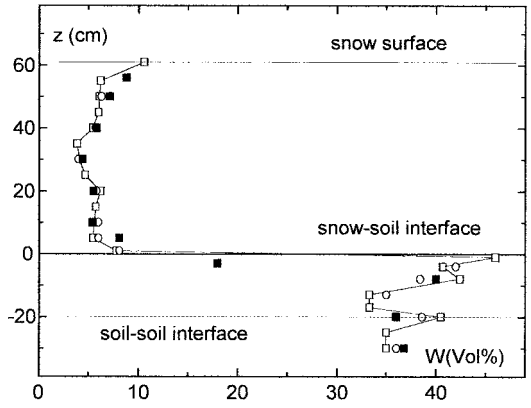

Fig. 10. Comparative measurement of a wetness profile at a snow-soil interface. Open circles: calorimetric (snow) and gravimetric (soil) measurements, open squares: capacitive probes; solid squares: monopole-probe.

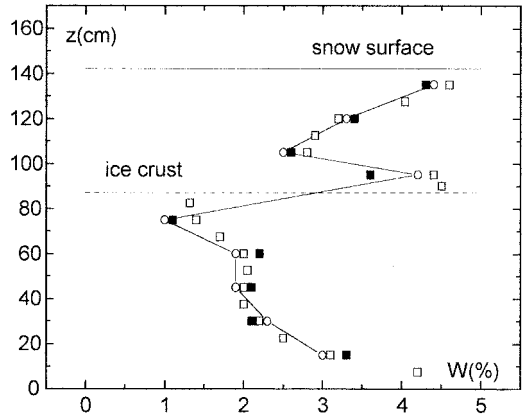

Fig. 11. Comparative measurement of a wetness profile of a snow cover with internal ice crusts. Open circles: calorimetric measurement; open squares: capacitive probes; solid squares: monopole-probe.

[12] wetness measurements. Fig. 9 shows Alpine ranker covered with 58 cm moderate wet old snow (density $\rho = 0.56$ g/cm^3; April 1995); soil temperature showed a small increase from 0 °C at the snow-soil boundary to +3 °C at a depth of 30 cm. Fig. 10 shows Alpine ranker covered with nearly 61 cm moderate wet to very wet old coarse-grained spring snow (June 1994). The increase in soil wetness at a soil depth of 20 cm correlates well with a change in soil texture: the first 20 cm represent the A_H-horizon (bulk density $\rho = 0.81$ g/cm^3), followed by the C-horizon (bulk density $\rho = 1.43$ g/cm^3) of this Alpine ranker. The marked increase in snow wetness near the soil surface (Figs. 8 and 9) may be due to a considerable change in hydraulic permeability which, in turn, affects water percolation through the snow cover. Fig. 11 shows moderate wet Alpine snow (March 1996), 142 cm in depth, and densities ranging from $\rho = 0.4$ g/cm^3 on top to $\rho \approx 0.54$ g/cm^3 at the bottom. The increase in snow wetness at the 87-cm level may be due to a high-density snow layer with a thin icy crust, more or less impermeable for percolating water. Wetness measurements with the monopole probe compared to standard techniques (freezing calorimetry [snow] and thermo-gravimetry [soil]) and capacitive probes show a satisfying agreement. In regions with low or only moderate variability in water distribution differences in the individual measurements are typically less than ±0.7% by volume for snow wetness, and less than ±2% by volume for soil wetness. However, due to the significantly larger sphere of influence of the monopole-probe, i.e., due to the lower spatial resolution, wetness detections using the monopole antenna

may deviate from the results obtained with the other techniques, especially in regions with a large gradient in wetness.

V. Conclusions

The monopole probe is a practical dielectric sensor well suited for *in situ* wetness measurements of different porous grainy geophysical materials as soils or snow. As antenna thickness is relatively small ($\approx$4 mm in diameter), the measurement is nearly nondestructive. Applied to snow, data evaluation is very simple: in the frequency range suggested for sensor operation (0.2–2 GHz) snow can be treated as a lossless dielectric material, and permittivity shows no significant variation with frequency. Liquid water measurement accuracy in snow is $\pm$0.7% by volume, and in soils $\pm$2%, which compares favorably to the intrinsic accuracies of freezing calorimetry and thermogravimetry, respectively. The actual accuracy of measurement, however, depends on a good contact of the probe to the surrounding medium: An air-gap has to be avoided around the center conductor—a region with high electric field strength—and this may be a problem in the case of a low-density low-wetness snow. So, for application of this sensor to snow the thickness of the center conductor should be increased to 6 or 10 mm, and should be designed as a thin hollow cylinder to minimize snow compaction. Applied to soils, data evaluation is more complicated, as both soil permittivity and total losses may vary with frequency. The formation of an air-gap around the probe has not been observed, so measurement accuracy is sufficient also for nearly dry soils.

References

[1] A. Denoth, "Snow liquid water measurements: Methods, instrumentation, results," in *Proc. Snowsymp'94*, Manali, India, 1994, pp. 150–153.

[2] J. R. Kendra, F. T. Ulaby, and K. Sarabandi, "Snow probe for *in situ* determination of wetness and density," *IEEE Trans. Geosci. Remote Sensing*, vol. 32, pp. 1152–1159, Nov. 1994.

[3] S. G. Ungar, R. Layman, J. E. Campbell, J. Walsh, and H. J. McKim, "Determination of soil moisture distribution from impedance and gravimetric measurements," *J. Geophys. Res.*, vol. 97, no. D17, pp. 18,969–18,977, 1992.

[4] T. Achammer, A. Giovannini, and A. Denoth, "Microwave X-K-band measurements on snow: Instrumentation and results," in *Proc. ISSW'94*, Snowbird, UT, Oct. 1994, pp. 676–679.

[5] S. C. Olson and M. F. Iskander, "A new *in situ* procedure for measuring the dielectric properties of low permittivity materials," *IEEE Trans. Instrum. Meas.*, vol. IM-35, pp. 2–6, Feb. 1986.

[6] A. Freundorfer, K. Iizuka, and R. Ramseier, "A method of determining electrical properties of geophysical media," *J. Appl. Phys.*, vol. 55, no. 1, pp. 218–222, 1984.

[7] D. W. Gooch, C. W. Harrison, Jr., R. W. P. King, and T. T. Wu, "Impedances of long antennas in air and dissipative media," *J. Res. Nat. Bur. Stand.*, vol. 67D, pp. 355–360, 1963.

[8] W. H. Gardener, "Water content" in *Methods of Soil Analysis*, A. Klute, Ed., 2nd ed. Madison, WI: Agronomy, 1987, pt. 1, no. 9.

[9] H. Eller and A. Denoth, "A capacitive soil moisture sensor," *J. Hydrology*, vol. 185, pp. 137–146, 1996.

[10] A. Denoth, H. Eller, and A. Gschnitzer, "Liquid water distribution at the snow-soil interface," in *Proc. ISSW'94*, Snowbird, UT, Oct. 1994, pp. 672–675.

[11] A. Denoth, "Snow dielectric measurements," *Adv. Space Res.*, vol. 9, no. 1, pp. 233–243, 1989.

[12] ——, "An electronic device for long-term snow wetness recording," *Ann. Glaciol.*, vol. 19, pp. 104–106, 1994.

[13] A. M. Thomas, "*In situ* measurement of moisture in soil and similar substances by 'fringe' capacitance," *J. Sci. Instrum.*, vol. 43, pp. 21–27, 1966.

[14] F. T. Ulaby, R. K. Moore, and A. K. Fung, Eds., *Microwave Remote Sensing.* Boston, MA: Artech House, 1986, vol. 3.

[15] P. Hoekstra and A. Delaney, "Dielectric properties of soils at UHF and microwave frequencies," *J. Geophys. Res.*, vol. 79, no. 11, pp. 1699–1708, 1974.

Correction to "GRSS Awards Presented at IGARSS'96"

In the above paper,[1] the citation to the 1996 IEEE **GRS-S Distinguished Achievement Award** was incorrect. It should read as follows.

> For pioneering contributions to microwave radiometric sensing from space.

Manuscript received August 13, 1997.
Publisher Item Identifier S 0196-2892(97)08036-4.

[1] W. Wiesbeck *et al.*, *IEEE Trans. Geosci. Remote Sensing*, vol. 35, pp. 797–800, July 1997.